nature medicine

ARTICLES

Identification of miR-145 and miR-146a as mediators of the 5q– syndrome phenotype

Daniel T Starczynowski[1,2], Florian Kuchenbauer[1], Bob Argiropoulos[1], Sandy Sung[1], Ryan Morin[1], Andrew Muranyi[1], Martin Hirst[1], Donna Hogge[1], Marco Marra[1], Richard A Wells[3], Rena Buckstein[3], Wan Lam[1,2], R Keith Humphries[1,4] & Aly Karsan[1,2]

5q– syndrome is a subtype of myelodysplastic syndrome characterized by severe anemia and variable neutropenia but normal or high platelet counts with dysplastic megakaryocytes. We examined expression of microRNAs (miRNAs) encoded on chromosome 5q as a possible cause of haploinsufficiency. We show that deletion of chromosome 5q correlates with loss of two miRNAs that are abundant in hematopoietic stem/progenitor cells (HSPCs), miR-145 and miR-146a, and we identify Toll–interleukin-1 receptor domain–containing adaptor protein (TIRAP) and tumor necrosis factor receptor–associated factor-6 (TRAF6) as respective targets of these miRNAs. TIRAP is known to lie upstream of TRAF6 in innate immune signaling. Knockdown of miR-145 and miR-146a together or enforced expression of TRAF6 in mouse HSPCs resulted in thrombocytosis, mild neutropenia and megakaryocytic dysplasia. A subset of mice transplanted with TRAF6-expressing marrow progressed either to marrow failure or acute myeloid leukemia. Thus, inappropriate activation of innate immune signals in HSPCs phenocopies several clinical features of 5q– syndrome.

Myelodysplastic syndrome (MDS), one of the most common hematopoietic malignancies, arises in primitive $CD34^+$ hematopoietic stem/progenitor cells[1–4]. MDS is characterized by ineffective hematopoiesis and dysplasia in one or more lineages of the bone marrow[5]. The paradoxical finding of normal or increased cellularity in the marrow in the context of peripheral blood cytopenias has been attributed to increased proliferation of hematopoietic cells that is counterbalanced by a simultaneous increase in apoptosis[6]. The majority of affected individuals either succumb to the consequences of marrow failure or progress to acute myeloid leukemia (AML)[5].

One of the most common subtypes of MDS, 5q– syndrome, is defined by an isolated interstitial deletion of chromosome 5q, refractory anemia, variable neutropenia and normal or high platelet counts associated with hypolobulated megakaryocytes[7]. Although the common deleted region (CDR) on chromosome 5q has been mapped to a 1.5-megabase region on band q33.1, distal breakpoints at band q33-q35 are more common, and, less often, deletions of the 5q arm are limited to a region distal to the CDR[8–10]. The CDR in 5q– syndrome contains several genes that are implicated in hematopoiesis[7]. Recently, the erythroid differentiation defect observed in 5q– syndrome has been attributed to the *RPS14* gene located within the CDR of chromosome 5q[11]. However, haploinsufficiency of *RPS14*, which encodes ribosomal protein S14, does not explain several of the other features of 5q– syndrome, namely, thrombocytosis associated with megakaryocytic dysplasia, neutropenia and clonal dominance (that is, replacement of the marrow by the malignant cells). Thus, loss of other genes probably contributes to the full manifestation of 5q– syndrome.

We postulated that loss of noncoding transcripts encoding miRNAs within the CDR may result in haploinsufficiency by loss of inhibition of their targets. miRNAs are small 21- to 25-nucleotide noncoding RNAs that post-transcriptionally repress specific messenger RNA targets through interaction with the 3′ untranslated region (UTR)[12]. We evaluated the expression of miRNAs located on chromosome 5q in MDS and found lower expression of miR-145 (5q33.1) and miR-146a (5q33.3) in individuals with MDS with deletion of the long arm of chromosome 5 (del(5q)). Concurrent loss of both miR-145 and miR-146a resulted in activation of innate immune signaling through elevated expression of their respective miRNA targets, TIRAP and TRAF6. Knockdown of miR-145 and miR-146a together or overexpression of TRAF6 in mouse HSPC recapitulated features of 5q– syndrome, such as increased platelet counts associated with dysplastic megakaryopoiesis and neutropenia, through cell-autonomous and cell-nonautonomous mechanisms.

RESULTS

Expression of miRNAs on chromosome 5q in MDS bone marrow

We performed massively parallel sequencing of small RNA libraries from five cell lines, with or without deletion of chromosome 5q (**Supplementary Fig. 1**), to a minimum depth of 4 million tags, to identify potential miRNAs on chromosome 5q. We found 25

[1]British Columbia Cancer Agency Research Centre, Vancouver, British Columbia, Canada. [2]Department of Pathology and Laboratory Medicine, University of British Columbia, Vancouver, British Columbia, Canada. [3]J.D. Crashley Myelodysplastic Syndrome Laboratory, Molecular and Cellular Biology, Sunnybrook Research Institute, Toronto, Ontario, Canada. [4]Department of Medicine, University of British Columbia, Vancouver, British Columbia, Canada. Correspondence should be addressed to A.K. (akarsan@bccrc.ca).

Received 20 May; accepted 30 September; published online 8 November 2009; doi:10.1038/nm.2054

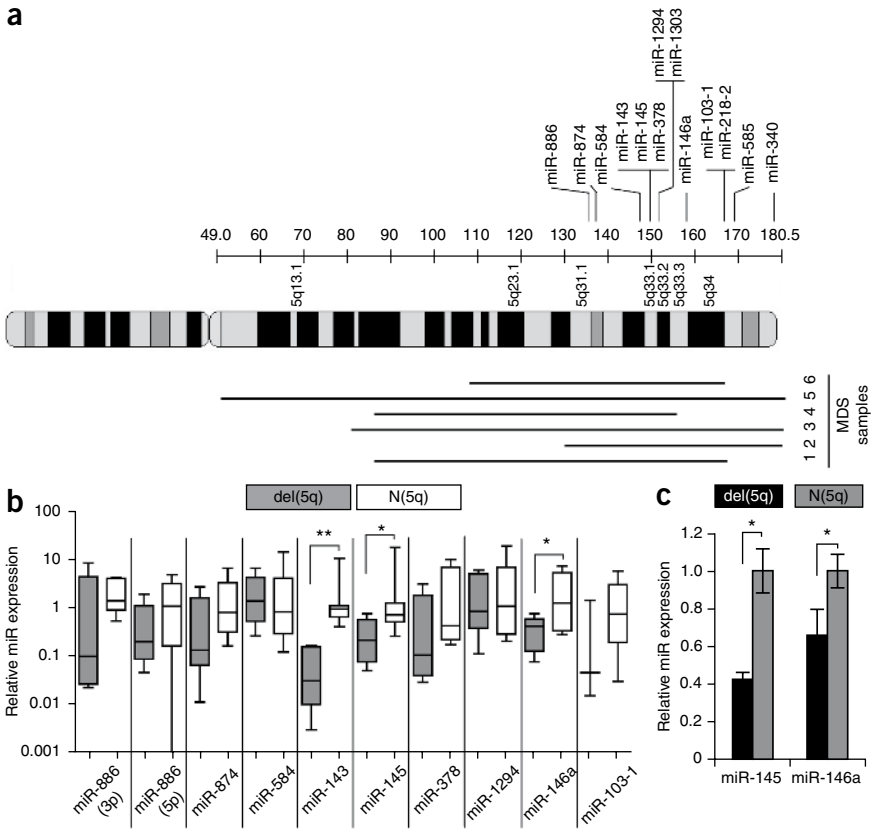

Figure 1 Expression analysis of miRNAs located on chromosome 5q in MDS. (**a**) A schematic showing chromosome 5q copy number deletions for human subjects with MDS (samples 1–6) as detected by array comparative genomic hybridization. The horizontal black lines below chromosome 5 indicate the extent of the deletion. The positions of all confirmed miRNAs telomeric to band q31 are indicated. (**b**) miRNA expression analysis, as performed by quantitative PCR (qPCR) on the marrow of six subjects with MDS with del(5q) and eight age-matched normal and MDS controls with a diploid chromosome arm 5q (N(5q)). The log expression levels (median and range of relative ΔC_t values) of each miRNA are shown by box-and-whisker plots. *P* values comparing del(5q) and diploid (5q) (N) miRNA ΔC_t values were calculated by the Student's *t*-test and corrected for multiple testing with the Benjamini and Hochberg test. $^*P < 0.05$; $^{**}P < 0.01$. (**c**) miRNA expression levels, as determined by qPCR for the indicated miRNAs and shown relative to the normal CD34$^+$ samples, from CD34$^+$ cells isolated from four normal (N(5q)) and three del(5q) MDS marrows. Data represent the means ± s.e.m. $^*P < 0.05$.

expressed miRNAs to reside on chromosome arm 5q, 13 of which are present in the most frequently deleted region between bands 5q31 and 5q35 (**Fig. 1a** and **Supplementary Table 1**). Analysis of these 13 miRNAs in bone marrow from subjects with MDS with del(5q) ($n = 6$), subjects with MDS with a normal karyotype ($n = 4$) and age-matched normal controls ($n = 4$) revealed ten miRNAs with substantial levels of expression in marrow (**Fig. 1a** and **Supplementary Table 2**). Quantitative RT-PCR (qRT-PCR) revealed three—miR-143 ($P = 0.01$), miR-145 ($P = 0.034$) and miR-146a ($P = 0.036$)—whose expression was significantly lower in MDS samples with del(5q) compared to MDS samples and controls with a normal karyotype (**Fig. 1b**).

As MDS is thought to arise from an HSPC within the CD34$^+$ compartment[2,3], we examined expression of miR-145 and miR-146a in CD34$^+$ cells from del(5q) marrows and normal CD34$^+$ control marrow. Expression of miR-145 ($P = 0.0047$) and miR-146a ($P = 0.04$) was significantly lower in CD34$^+$ cells from del(5q) marrow cells compared to normal CD34$^+$ controls (**Fig. 1c**), suggesting that these two miRNAs may have a pathogenic role in 5q– syndrome.

Knockdown of miR-145 and miR-146a mimics 5q– syndrome

To determine whether miR-145 and miR-146a contribute to features of 5q– syndrome, we stably knocked down both miR-145 and miR-146a in mouse HSPCs by retrovirus-mediated overexpression of miR-145 and miR-146a target sequences, which were engineered together into the 3′ UTR of yellow fluorescent protein (YFP; the resulting construct is referred to as 'miR decoy') (**Fig. 2a**,**b**)[13,14]. To examine the hematopoietic effects of the loss of miR-145 and miR-146a, we transplanted lethally irradiated C57BL/6 mice with 5×10^5 marrow cells transduced with the miR decoy construct or vector alone, along with 2×10^5 wild-type competitor marrow cells. We generated this chimeric marrow representing a mixture of transduced (YFP$^+$) and nontransduced (YFP$^-$) cells to mimic the chimerism often seen in the marrows of individuals with 5q– syndrome[15,16]. At 8 weeks after marrow transplant, blood counts revealed significant thrombocytosis (platelets: 1,215 ± 24 versus 1,019 ± 76 × 10^9 cells per l, $P = 0.005$) and variable neutropenia (granulocytes: 2.9 ± 0.3 versus 3.7 ± 0.5 × 10^9 cells per l, $P = 0.08$) in miR decoy–transduced mice ($n = 13$) compared to vector controls ($n = 9$) (**Fig. 2c**, **Table 1** and **Supplementary Table 3**). Myeloid activity was suppressed in miR decoy–transduced mouse marrows, as indicated by lower numbers of clonogenic progenitors (**Fig. 2d**). In contrast, there was enhanced megakaryopoiesis in miR decoy–transduced mouse marrows, as noted by increased megakaryocyte colony formation ($P = 0.004$) (**Fig. 2e**). As in 5q– syndrome, hypolobated megakaryocytes were obvious in miR decoy–chimeric mice (**Fig. 2f**).

The hypolobated morphology was confirmed by DNA ploidy analysis of CD41$^+$ megakaryocytes in the marrow, consistent with reduced endoreduplication in the miR decoy–chimeric marrows (41.0% ± 6.2% ≤ 4*n* ploidy with miR decoy marrow versus 19.7% ± 0.7% ≤ 4*n* with vector marrow, $P = 0.013$) (**Fig. 2g**). We observed a similar reduction in DNA ploidy when we used CD61 as the megakaryocytic marker (**Supplementary Fig. 2**). Thus, loss of miR-145 and miR-146a results in hematopoietic abnormalities reminiscent of 5q– syndrome, including thrombocytosis, characteristic dysmegakaryopoiesis and variable neutropenia.

miR-145 and miR-146a target TIRAP and TRAF6, respectively

According to published online algorithms[17], over 500 genes are predicted targets of miR-145 and miR-146a. To identify signaling pathways potentially impinged by these two miRNAs, we analyzed the predicted mRNA targets with Ingenuity Pathways Analysis. Of the predicted networks identified, the innate immune response pathway was very highly ranked ($P = 1 \times 10^{-36}$) (**Supplementary Fig. 3a**). Several signaling molecules in the Toll-like receptor (TLR) pathway

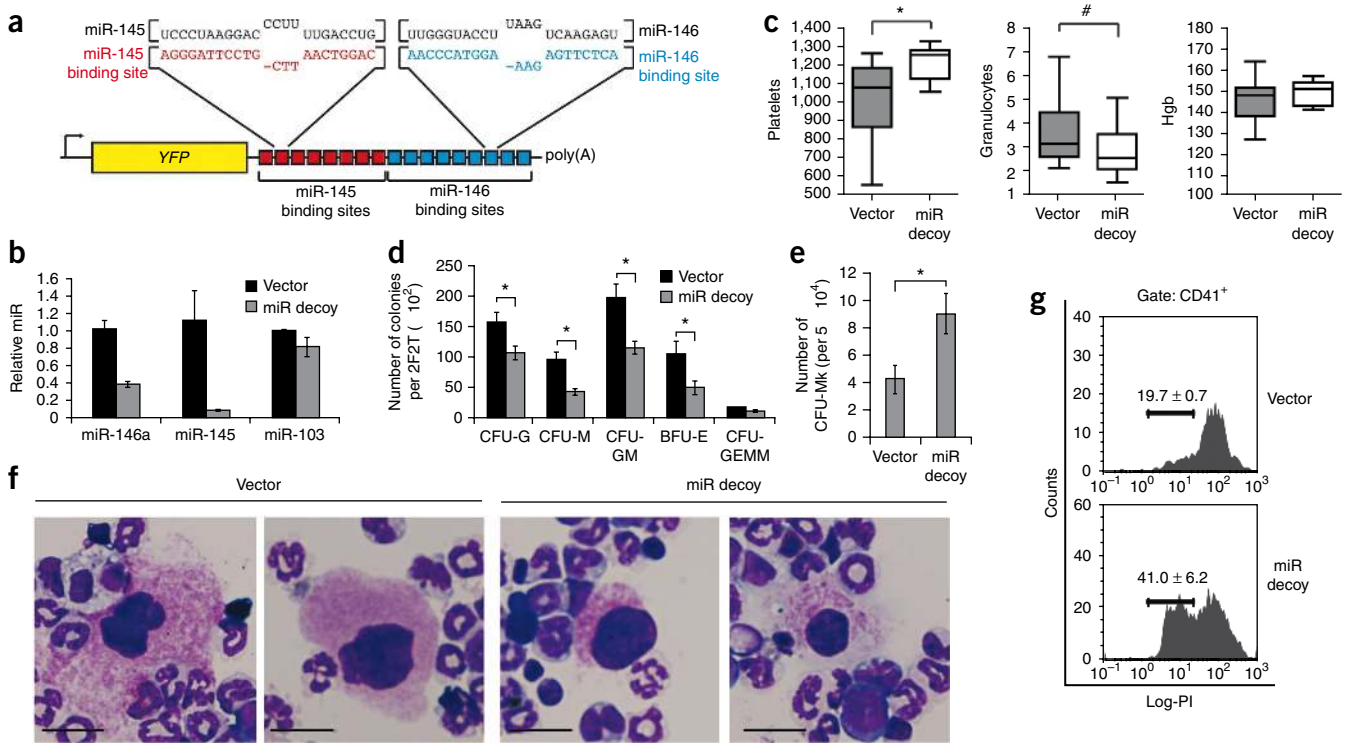

Figure 2 Stable knockdown of miR-145 and miR-146a in mouse marrow results in a 5q–like syndrome. (**a**) Schematic representation of the miR decoy. Eight miR-145 and nine miR-146a target sequences were inserted into the 3′ UTR of a *YFP* reporter gene driven by the cytomegalovirus promoter. Poly(A), polyadenylation tail. Dashes indicate that there is no nucleotide at that position in the sequence. (**b**) Endogenous expression of miR-145, miR-146a and miR-103, as determined by qPCR, in marrow cells transduced with miR decoy or vector. Data shown are means ± s.e.m. of four independent experiments. (**c**) Blood counts of platelets (× 10^9 per l), granulocytes (× 10^9 per l) and hemoglobin (Hgb) (g l^{-1}), in miR decoy–chimeric ($n = 13$) and vector-chimeric ($n = 9$) mice at 8 weeks from two independent experiments, shown as box-and-whisker plots. (**d**) Numbers of colony-forming cells (CFCs) from marrow of four vector-chimeric and four miR decoy–chimeric mice from two independent experiments collected at approximately 3.5 months after transplant. The number of colonies in two femurs and two tibias (2F2T) per mouse are shown. CFU, colony-forming unit; G, granulocyte; M, macrophage and monocyte; BFU, burst-forming unit; E, erythroid. (**e**) Numbers of megakaryocyte CFUs (CFU-Mk) from three vector-chimeric and three miR decoy–chimeric mice, collected at approximately 3.5 months after transplant. (**f**) Wright-Giemsa–stained marrow cytospins from vector- and miR decoy–chimeric mice. Images are representative of three mice per group. Scale bars, 10 μm. (**g**) Ploidy analysis of $CD41^+$ megakaryocytes, as determined by measuring propidium iodide (PI) incorporation using flow cytometry. Shown is a representative plot from three separate mice. The data represent the mean percentage of cells ± s.e.m. with DNA content ≤ 4*n*. $^*P < 0.01$; $^{\#}P = 0.08$.

were predicted to be targeted, including TIRAP (by miR-145) and TRAF6 (by miR-146a) (**Supplementary Fig. 3b**).

To test whether miR-145 and miR-146a directly target the 3′ UTRs of TIRAP and TRAF6, respectively, we performed luciferase assays using 3′ UTR sequence fragments containing the predicted targets of each of the two miRNAs inserted separately downstream of a luciferase reporter, as previously described[18]. As controls, we analyzed TIRAP and TRAF6 3′ UTRs with mutated versions of the predicted miRNA binding sites (MutTIRAP 3′ UTR and MutTRAF6 3′ UTR). Transient transfection into HEK293 cells with the TIRAP 3′ UTR construct together with miR-145 yielded a 60% decrease in reporter activity compared to vector-transfected cells, which was abrogated when the predicted miR-145

Table 1 Characterization of the peripheral blood of transplanted mice

	Donor BM	WBC (× 10^9 per l)	Granulocytes (× 10^9 per l)	RBC (× 10^{12} per l)	Hgb (g l^{-1})	Hct (%)	Plt (× 10^9 per l)	MCV (μm^3)	RDW (%)
Vector	Wild type	9.6	3.7	10	146	44.4	1,019	44.3	15.5
miR decoy	Wild type	8.6	2.9	10.3	149	45.5	1,215	44.5	15.4
P value		0.17	0.08	0.24	0.18	0.17	0.0052	0.43	0.30
MIY	Wild type	11.6	4.9	12.4	145	56.1	384.2	44.8	14.9
TRAF6	Wild type	7.4	3.2	10.6	127	48.2	558.9	45.5	16.2
P value		0.00012	0.003	0.041	0.08	0.05	0.018	0.28	0.024
MIY	*Il6*$^{-/-}$	8.2	2.6	10.0	147	46.5	438.6	47.1	14.9
TRAF6	*Il6*$^{-/-}$	8.1	3.4	9.5	139	43.8	470.7	45.9	15.0
P value		0.45	0.08	0.35	0.26	0.26	0.50	0.08	0.81

WBC, white blood cell; RBC, red blood cell; Hgb, hemoglobin; Hct, hematocrit; Plt, platelet; MCV, mean corpuscular volume; RDW, red cell distribution width. Further details are listed in **Supplementary Tables 3**, **4** and **7**. *P* values were calculated by the Student's *t*-test.

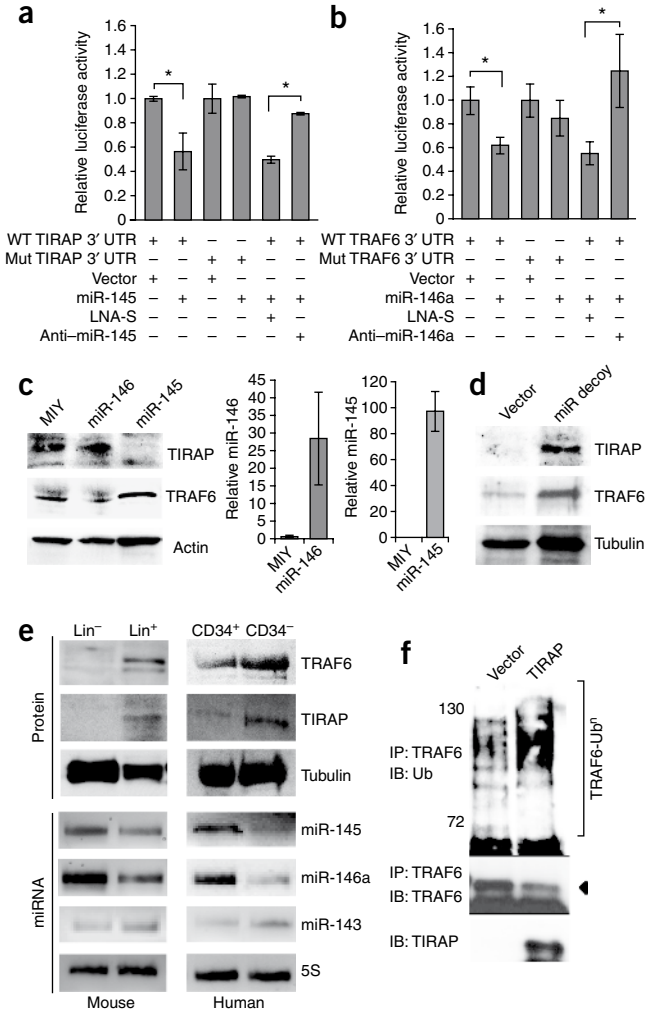

Figure 3 TIRAP and TRAF6 are targets of miR-145 and miR-146a, respectively. (**a**) Luciferase reporter assays performed with firefly luciferase under control of the TIRAP 3′ UTR (wild type (WT) or mutant (Mut)), control *Renilla* luciferase and the indicated miRNA. The firefly luciferase values were normalized for transfection with *Renilla* luciferase activity, and data are presented relative to the vector control assigned a value of 1. The mean ± s.e.m. of three independent experiments is shown. $^*P < 0.05$. (**b**) Luciferase reporter assays performed with firefly luciferase under control of the TRAF6 3′ UTR (wild type (WT) or mutant (Mut)), control *Renilla* luciferase and the indicated miRNA. The firefly luciferase values were normalized for transfection with *Renilla* luciferase activity, and data are presented relative to the vector control assigned a value of 1. The mean ± s.e.m. of three independent experiments is shown. $^*P < 0.05$. (**c**) Mouse marrow cells transduced with miR-146a, miR-145, or vector control (MIY) were sorted for YFP expression and analyzed for protein (immunoblot, left, representative of two independent experiments) and miRNA expression normalized to *5S* RNA expression (qPCR, right). Data shown for miRNA expression are mean ± s.e.m. of three independent experiments. (**d**) Lysates of mouse marrow cells transduced with miR decoy or vector control immunoblotted with antibodies against TIRAP, TRAF6 and tubulin. Results are representative of two independent experiments. (**e**) Immunoblotting and RT-PCR analysis of normal mouse and human hematopoietic cells fractionated into primitive (Lin⁻ (mouse) or CD34⁺ (human)) or committed (Lin⁺ (mouse) or CD34⁻ (human)) populations. Immunoblotting was performed for TRAF6 and TIRAP on protein fractions, and small RNAs were collected and analyzed by RT-PCR using miRNA-specific primers. Data are representative of two independent experiments. (**f**) Immunoblots (IB) for ubiquitin (Ub), TRAF6 and TIRAP of the immunoprecipitation (IP) or pre-IP lysate of HEK293 cells transfected with TIRAP or vector control constructs. The size of the proteins in kDa is indicated on the left. Arrowhead points to the TRAF6 band. Data are representative of two independent experiments.

binding site was mutated (**Fig. 3a**). As previously reported, miR-146a reduced reporter activity of the wild-type, but not mutated, TRAF6 3′ UTR by 45% compared to the empty vector control (**Fig. 3b**)[18]. To confirm that the miRNAs regulate the protein expression of their respective targets in bone marrow cells, we retrovirally transduced mouse HSPCs with miR-145 or miR-146a and examined protein expression by immunoblotting. miR-145 repressed TIRAP protein expression, and miR-146a repressed TRAF6 protein expression (**Fig. 2c**).

To confirm that depletion of these miRNAs increases TIRAP and TRAF6 protein expression, we examined lysates from mouse HSPCs transduced with both of the miR decoy constructs (**Fig. 2b**) and found an increase in TIRAP and TRAF6 protein abundance (**Fig. 3d**). Furthermore, in normal human and mouse marrow, there was an inverse correlation between miR-145 and TIRAP expression and between miR-146a and TRAF6 expression: there was relatively high expression of miR145 and miR146a in primitive CD34⁺ and Lin⁻ populations compared to CD34⁻ and Lin⁺ populations, and for TIRAP and TRAF6 the reverse was true (**Fig. 3e**).

Overexpression of TRAF6 mimics features of 5q– syndrome

TRAF6 is an E3 ubiquitin ligase that catalyzes self-directed Lys63-linked polyubiquitination, resulting in downstream activation of nuclear factor-κB (NF-κB)[19]. To confirm and extend previous data showing that TIRAP interacts with TRAF6 to activate NF-κB[20], we transfected TIRAP into HEK293 cells, immunoprecipitated TRAF6 and directly showed TRAF6 activation by TIRAP, as indicated by increased polyubiquitination of TRAF6 (ref. 21) (**Fig. 3f**). Furthermore, TIRAP activated NF-κB in the presence of endogenous TRAF6 but concurrent expression of a dominant-negative TRAF6 construct abrogated TIRAP-induced NF-κB activation (**Supplementary Fig. 3c**), confirming that TIRAP activates NF-κB through TRAF6. In addition, knockdown of miR-145 or miR-146a also activated the NF-κB pathway (**Supplementary Fig. 3d**,**e**). These findings suggest that partial loss of miR-145, miR-146a or both results in increased signaling through TRAF6, and imply that enforced expression of TRAF6 should mimic the effects seen by loss of either or both of these miRNAs.

To determine whether ectopic activation of innate immune signaling in HSPCs is sufficient to mimic the aspects of 5q– syndrome evoked by loss of miR-145 and miR-146a, we examined the hematopoietic effects of enforced TRAF6 expression. We transplanted lethally irradiated C57BL/6 mice with 1×10^6 marrow cells retrovirally transduced with TRAF6 (with an internal ribosomal entry site–linked YFP) or vector alone (murine stem cell virus–internal ribosomal entry site–YFP (MIY)) along with 2×10^5 of nontransduced marrow cells. Immunoblotting confirmed TRAF6 protein expression *in vitro* and *in vivo* at levels similar to those seen after miR-146a knockdown (**Fig. 4a**). By 12 weeks after marrow transplantation and continuing on to 24 weeks, we observed significant neutropenia ($P = 0.0001$) and thrombocytosis ($P = 0.018$) in TRAF6-transduced mice ($n = 18$) compared to MIY-transduced mice ($n = 13$) (**Fig. 4b**, **Table 1** and **Supplementary Table 4**). As with loss of miR-145 and miR-146a, ectopic TRAF6 expression suppressed marrow myeloid progenitor activity (**Fig. 4c**). Flow cytometry revealed higher proportions of Mac1⁺Gr1⁻ cells at the expense of Mac1⁺Gr1⁺ cells in chimeric marrows of TRAF6-transduced compared to MIY-transduced mice, suggesting an altered myeloid differentiation program (**Supplementary Fig. 4**).

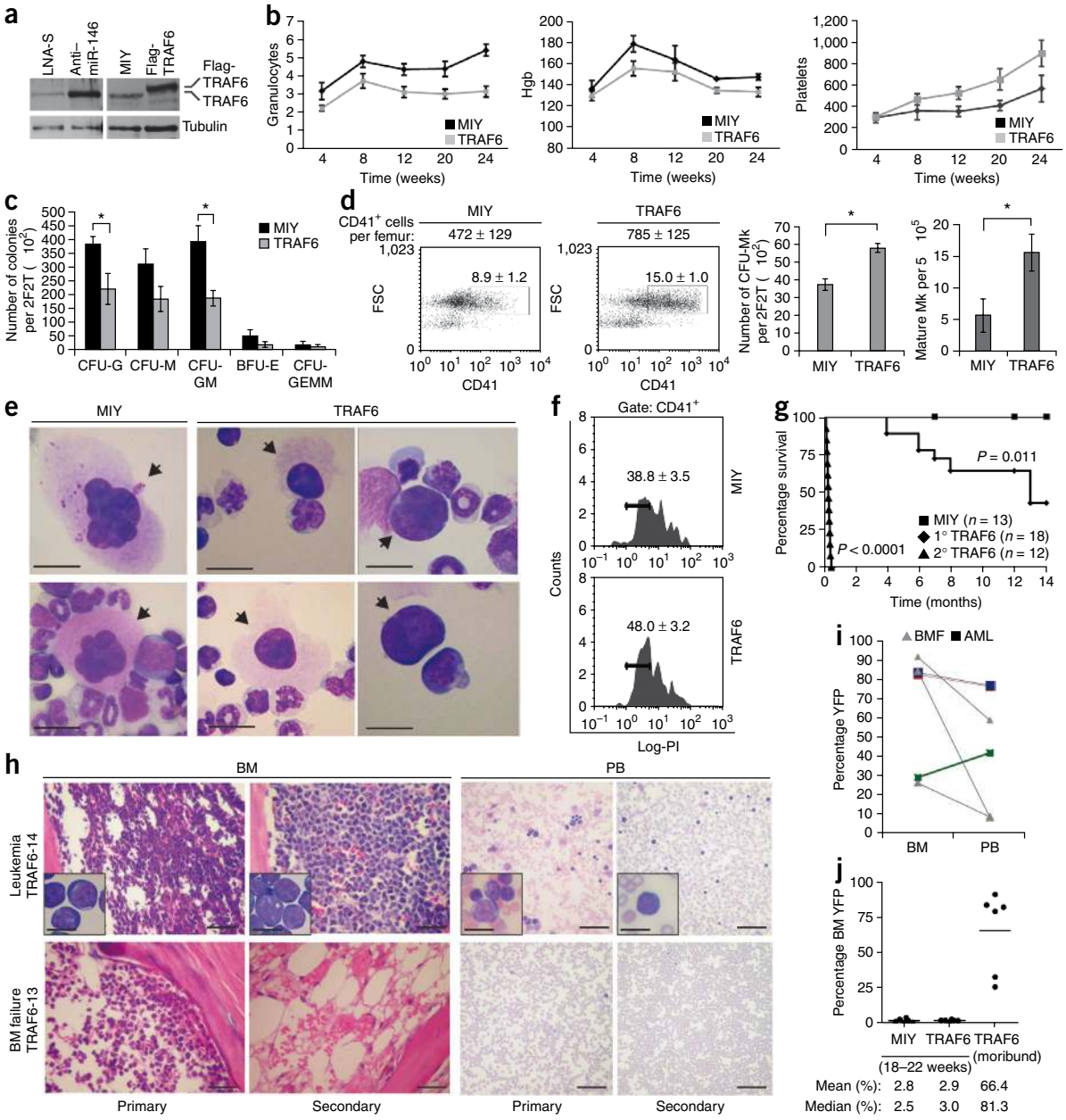

Figure 4 TRAF6 expression in mouse marrow results in a syndrome similar to the 5q– syndrome and progression to either marrow failure or AML. (**a**) Immunoblot analysis for TRAF6 expression performed on Flag-TRAF6–transduced or MIY-transduced marrow cells before transplantation, as well as on marrow cells transfected with anti–miR-146 or the scrambled control oligonucleotide (LNA-S) (as in **Supplementary Fig. 11b**,**c**). Data are representative of two independent experiments. (**b**) Granulocyte counts (× 10^9 per l), hemoglobin (Hgb) (g l^{-1}) and platelet counts (× 10^9 per l) in TRAF6-transduced ($n = 18$) and MIY-transduced ($n = 13$) mice from three independent experiments. Error bars represent s.e.m. (**c**) Marrow CFC assays performed approximately 6 months after marrow transplant. Data show mean progenitor number ± s.e.m. from six mice. $^*P < 0.05$. (**d**) Left, representative flow cytometry dot plots of marrow cells stained with CD41-specific antibody. The percentage of cells in the gated region represents the mean ± s.e.m. of three mice in each group. The mean numbers ± s.e.m. of $CD41^+$ cells per femur are shown above each dot plot. Middle, mean megakaryocyte progenitor numbers (CFU-Mk) ± s.e.m. per two femurs and two tibias (2F2T) approximately 6 months after marrow transplant from three mice. $^*P < 0.05$. Right, megakaryocyte (Mk) counts from Wright-Giemsa–stained cytospin preparations from MIY-transfected ($n = 3$) and TRAF6-transfected ($n = 3$) mice. Data shown are the means ± s.e.m. $^*P < 0.05$. (**e**) Wright-Giemsa–stained marrow cytospins showing representative megakaryocyte morphology (arrows) from six different mice each in the MIY and TRAF6 groups. Scale bars, 10 μm. (**f**) Megakaryocyte ($CD41^+$) ploidy, as determined by PI incorporation using flow cytometry. Shown is a representative plot from three independent experiments with marrow from a single mouse in each experiment. Numbers represent percentage of cells ± s.e.m. in the gated region with DNA content ≤ 4*n*. (**g**) Kaplan-Meier survival curves for primary transplanted mice reconstituted with marrow transduced with MIY ($n = 13$) or TRAF6 ($n = 18$) from three independent experiments or for secondary transplanted mice from TRAF6-transduced ($n = 12$) marrow in two independent experiments. (**h**) H&E-stained femur sections and Wright-Giemsa–stained bone marrow (BM) or peripheral blood (PB) representative of six different mice in each group. Scale bars, 50 μm. The insets are magnified views of the same marrows or blood; the scale bars in the insets represent 10 μm. (**i**) YFP expression, determined by flow cytometry at the time of death, by bone marrow and blood cells from moribund TRAF6-transduced mice. BMF, bone marrow failure. $n = 3$ mice for BMF and $n = 3$ mice for AML. (**j**) Proportion of MIY-transduced marrow cells ($n = 6$) or TRAF6-transduced marrow cells ($n = 6$) in mice 18 and 22 weeks after transplant or moribund TRAF6-transduced mice ($n = 6$), as determined by the percentage of YFP^+ cells by flow cytometry. Horizontal lines represent the means of the values obtained.

Similarly to marrow lacking miR-145 and miR-146a, the marrow of TRAF6-chimeric mice showed increased megakaryopoiesis, as indicated by a higher proportion of CD41$^+$ cells (15.0% ± 1.0%) compared to MIY-transduced mice (8.9% ± 1.2%, $P = 0.019$) (**Fig. 4d**) and an approximately 50% increase in megakaryocyte colony formation ($P = 0.017$) (**Fig. 4d**). Morphological examination revealed a threefold increase in megakaryocyte numbers in TRAF6-transduced marrows, as well as megakaryocyte clusters in the spleen (**Fig. 4d** and

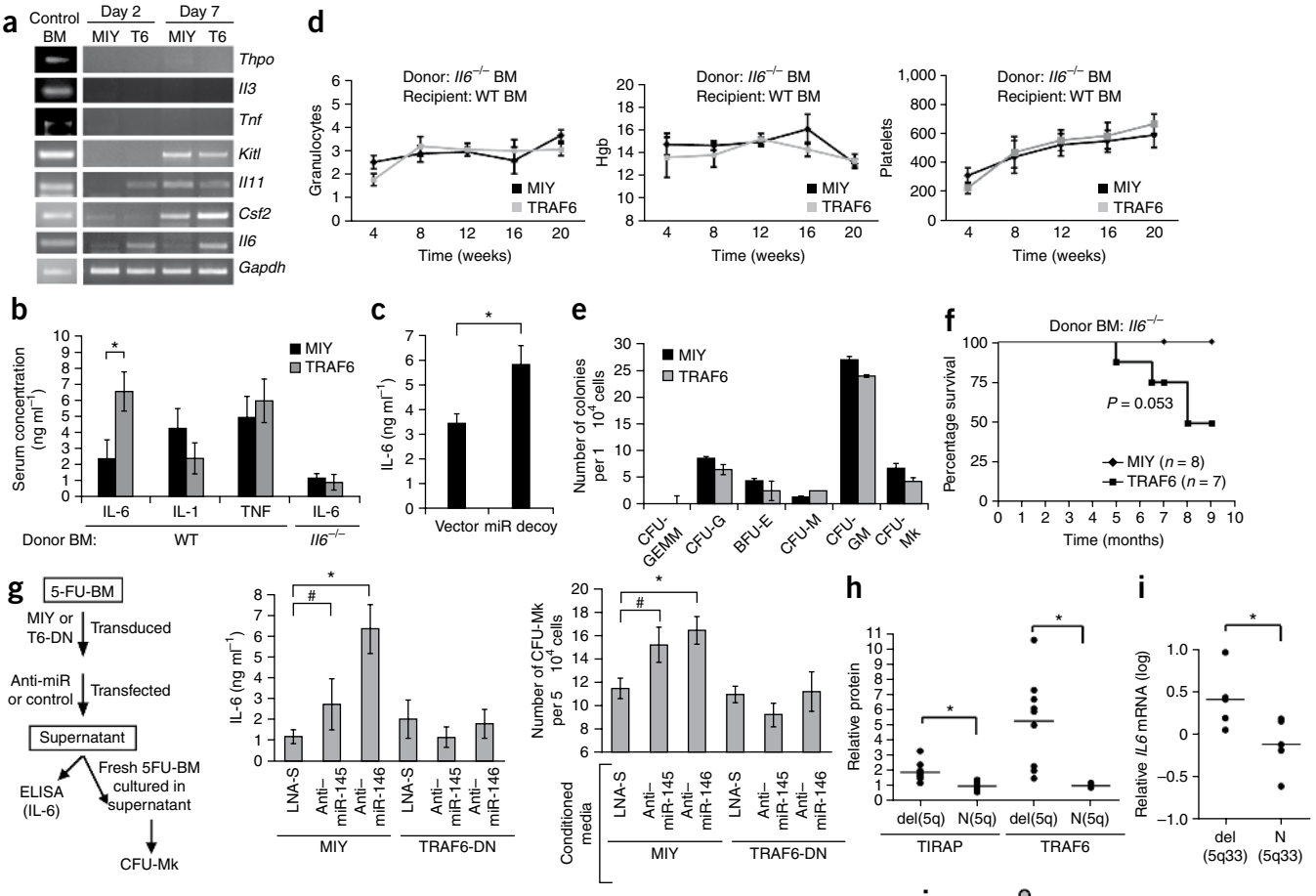

Figure 5 Paracrine effects of IL-6 contribute to hematopoietic defects in TRAF6-transduced mice. (**a**) Semi-quantitative RT-PCR analysis for the indicated genes performed on RNA harvested from fresh marrow from wild-type mice (control BM) or MIY- or TRAF6 (T6)-expressing marrow cells, 2 or 7 d after flow sorting. Data are representative of two independent experiments. *Thpo*, thrombopoietin; *Tnf*, tumor necrosis factor; *Kitl*, Kit ligand; *Csf2*, colony-stimulating factor-2; *Gapdh*, glyceraldehyde 3-phosphate dehydrogenase. (**b**) Serum ELISA was performed for the indicated cytokines 16–28 weeks after transplantation into lethally irradiated wild-type recipient mice using MIY-transduced wild-type or *Il6*$^{-/-}$ marrow donor cells ($n = 6$ for each group) or TRAF6-transduced wild-type or *Il6*$^{-/-}$ marrow donor cells ($n = 6$ for each group). Data shown are means ± s.e.m. $^*P < 0.05$. (**c**) Serum ELISA performed for IL-6 on mice at 8–12 weeks after marrow transplantation of wild-type marrow donor cells transduced with vector ($n = 4$) or miR decoy ($n = 5$) into lethally-irradiated wild-type recipient mice. Data shown are means ± s.e.m. $^*P < 0.05$. (**d**) Granulocyte counts (×10^9 per l), hemoglobin concentration (Hgb) (g l^{-1}) and platelet counts (×10^9 per l) of TRAF6-transduced ($n = 7$) and MIY-transduced ($n = 8$) mice from two independent experiments. MIY or TRAF6-transduced *Il6*$^{-/-}$ marrow cells were transplanted along with wild-type helper cells into lethally irradiated wild-type recipient mice. Data are means ± s.e.m. (**e**) CFC assays performed approximately 6 months after transplantation using *Il6*$^{-/-}$ marrow transduced with MIY ($n = 3$) or TRAF6 ($n = 3$). Data show mean progenitor number ± s.e.m. (**f**) Kaplan-Meier survival curves for mice reconstituted with *Il6*$^{-/-}$ marrow donor cells transduced with MIY ($n = 8$) or TRAF6 ($n = 7$) mice from two independent experiments. (**g**) Left, schematic outlining the experimental scheme: miRNA knockdown with LNA oligonucleotides targeting miR-145 or miR-146a, or with a scrambled control (LNA-S) oligonucleotide, was performed in the presence or absence of TRAF6 blockade with a TRAF6 dominant-negative (T6-DN) construct or control vector (MIY), respectively. Middle, IL-6 concentrations in the marrow cell supernatants under the various conditions, as determined by ELISA (middle panel). Right, megakaryocyte progenitor assays (CFU-Mk) of the same supernatants. Data shown are means ± s.e.m. of six experiments. $^*P < 0.05$; $^\#P = 0.07$. (**h**) Protein expression of TRAF6 and TIRAP relative to β-actin, as determined by densitometry of immunoblots of marrow from subjects with MDS with del(5q) ($n = 9$) or normal subjects and subjects with MDS without del(5q) (N5q) ($n = 8$). $^*P < 0.05$. (**i**) RT-PCR of *IL6* mRNA, as performed on marrow from five subjects with MDS with del(5q) encompassing the region at band q33 and five subjects with MDS diploid at band 5q33. $^*P < 0.05$. (**j**) Model of del(5q) MDS in the context of miRNA loss. IRAK1, interleukin-1 receptor–associated kinase-1; MyD88, myeloid differentiation factor-88; Ub, ubiquitin.

Supplementary Fig. 5a). CD41$^+$ megakaryocytes showed reduced DNA ploidy and were hypolobated, and there was an increase in the frequency of micromegakaryocytes (megakaryocytes no bigger than proerythroblasts) in TRAF6-chimeric marrow compared to vector control marrow (48.0% ± 3.1% versus 38.8% ± 3.5% of cells ≤ 4*n*, $P = 0.0037$) (**Fig. 4e**,**f**). Thus, enforced expression of TRAF6 results in hematopoietic abnormalities similar to those found with loss of miR-145 and miR-146, including dysplastic megakaryopoiesis, thrombocytosis and mild neutropenia.

Overexpression of TRAF6 induces AML or marrow failure

Individuals with 5q– syndrome may progress either to marrow failure or AML[22]. We monitored the TRAF6-chimeric mice for up to 14 months and found that, starting at 5 months, approximately a third (7 of 18) of these mice began to succumb to marrow failure or AML (**Fig. 4g** and **Supplementary Fig. 5**). Three of the seven mice progressed to marrow failure, and the remaining four mice developed AML (**Supplementary Tables 5** and **6**). Marrow failure was characterized by severe anemia and thrombocytopenia despite normocellular marrows (**Fig. 4h**, **Supplementary Fig. 5b** and **Supplementary Tables 5** and **6**). Consistent with ineffective hematopoiesis, the YFP$^+$ cells of mice with marrow failure were less abundant in the blood as compared to the marrow (**Fig. 4i**). Leukemic mice had marrow replacement by blast cells, circulating blast cells and splenomegaly (**Fig. 4h**, **Supplementary Figs. 5c–f** and **Supplementary Tables 5** and **6**). We found YFP$^+$ cells at approximately equal proportions in the marrow and blood of leukemic mice, consistent with the blast cells being of donor origin (**Fig. 4i**).

There was a massive increase in the proportion of YFP$^+$ cells in the marrow of the moribund mice compared to marrow aspirates from six chimeric mice that were still healthy 18 to 22 weeks after transplant, suggesting that AML or marrow failure is associated with an increase in the number of TRAF6-expressing cells, that is, clonal dominance (**Fig. 4j**). The increase in the proportion of YFP$^+$ cells reflects increased apoptosis in the untransduced (YFP$^-$), but not in the transduced (YFP$^+$), marrow fraction of TRAF6-transduced mice (13.6% ± 3.4%) compared to MIY-transduced mice (5.4% ± 2.7%), as detected by annexin V staining 18 to 22 weeks after transplant (**Supplementary Fig. 6a**). Indeed, there was significant protection of TRAF6-expressing (YFP$^+$) Lin$^-$ progenitor cells compared to the untransduced (YFP$^-$) Lin$^-$ cells in the same marrow ($P = 0.006$) (**Supplementary Fig. 6b**). In *ex vivo* experiments, loss of miR-145 or miR-146a protected marrow cells from apoptosis in culture in a TRAF6-dependent manner (**Supplementary Fig. 6c–f**). The marrows of TRAF6-chimeric mice that remained healthy over a period of 12 months did not show an increase in the primitive Lin$^-$Sca1$^+$ c-Kit$^+$ (LSK) population, and the marrows of TRAF6-chimeric mice that underwent bone marrow failure showed varying Sca1 and c-Kit expression suggesting an aberrant primitive hematopoietic population (**Supplementary Fig. 7a**,**b**). In contrast, the marrows of TRAF6-chimeric mice that developed AML showed a homogeneous Lin$^-$ cell population that was c-Kit^{low} and Sca1^{dim} (**Supplementary Fig. 7b**,**c**). Taken together, these findings suggest that TRAF6 expression protects HSPCs against apoptosis while promoting cell death in the coexisting wild-type HSPC. These findings are also consistent with findings from humans with MDS, in whom apoptosis has been reported to involve primarily the coexisting normal hematopoietic population[6].

We next transplanted marrow cells obtained from primary TRAF6-transduced mice succumbing either to marrow failure or AML into secondary recipients. All transplanted mice died rapidly from marrow failure or leukemia, congruent with the primary disease (**Fig. 4g**,**h** and **Supplementary Fig. 8**). Secondary recipients receiving cells from a mouse with AML showed blast cell–infiltrated marrows, large numbers of circulating blast cells and hepatosplenomegaly with heavily infiltrated livers and spleens (**Fig. 4h** and **Supplementary Fig. 8a–c**). In contrast, secondary recipients receiving cells from a mouse with marrow failure showed engraftment failure, with peripheral cytopenias and hypocellular marrows, despite concurrent transplantation of helper cells (**Fig. 4h** and **Supplementary Fig. 8a**,**b**). Hence, mice transplanted with TRAF6-expressing marrow cells progress from a 5q– syndrome–like disease to a transplantable acute leukemia or marrow failure.

TRAF6 induces cell nonautonomous effects through IL-6

Examination of YFP expression in the peripheral blood revealed a gradual depletion of YFP$^+$ cells in the blood of both TRAF6-transduced and miR decoy–transduced mice over the first few months after transplantation (**Supplementary Fig. 9a**). However, the percentage of YFP$^+$ peripheral cells did not correlate with the level of thrombocytosis in either the TRAF6- or miR decoy–chimeric marrows (**Figs. 2c** and **4b** and **Supplementary Fig. 9b**). As dysplastic changes in 5q– syndrome are found both in cells with del(5q) as well as in cells lacking del(5q)[15], this discordance suggests cell nonautonomous effects resulting from increased TRAF6 expression. To determine whether cell-nonautonomous effects might account for the increased and dysplastic megakaryopoiesis observed in mice transplanted with TRAF6-transduced marrows, we examined the proportion of YFP$^+$ and YFP$^-$ cells in the CD41$^+$ megakaryocytic fraction of marrows from TRAF6-chimeric and MIY-chimeric mice. These proportions were similar (**Supplementary Fig. 9c**), implying a cell-nonautonomous basis for the megakaryocytic phenotype. Consistent with this idea, we observed hypolobulated megakaryocytes in both the transduced (YFP$^+$) and nontransduced (YFP$^-$) cell populations of marrow from TRAF6-transduced mice (**Supplementary Fig. 9d**).

To elucidate a possible paracrine mechanism of thrombocytosis in the TRAF6-transduced mice, we investigated the expression of cytokines and growth factors involved in megakaryopoiesis. After transduction of TRAF6 into mouse HSPCs, only *Il6* (encoding interleukin-6 (IL-6) showed both rapid induction and persistent elevation until day 7 (**Fig. 5a**). IL-6 is a potent activator of megakaryocyte survival, differentiation and platelet formation[23]. We examined circulating amounts of IL-6 in the serum of TRAF6-chimeric mice and found a 2.8-fold increase ($P = 0.023$) of IL-6, but not of IL-1β or tumor necrosis factor, compared to MIY-transduced mice (**Fig. 5b**). Similarly, miR decoy–chimeric mice showed an approximately two-fold increase ($P = 0.03$) in serum IL-6 concentrations compared to control mice (**Fig. 5c**). The TRAF6-transduced donor marrow cells in the transplanted mice seem to be producing the IL-6 leading to increased serum IL-6 concentrations, because these concentrations were not increased in lethally irradiated wild-type mice transplanted with TRAF6-transduced marrow from *Il6*$^{-/-}$ mice (**Fig. 5b**).

We next determined whether IL-6 contributes to the TRAF6-mediated hematopoietic defects by transplanting TRAF6-transduced marrow from *Il6*$^{-/-}$ mice into lethally irradiated wild-type mice. Blood counts revealed that MIY-chimeric ($n = 8$) and TRAF6-chimeric ($n = 7$) mice had similar granulocyte counts ($P = 0.08$), hemoglobin levels ($P = 0.26$), platelet counts ($P = 0.5$) and marrow progenitor activity (**Fig. 5d**,**e**, **Table 1** and **Supplementary Table 7**). However, when followed for 11 months, three of seven TRAF6-transduced mice,

but none of the MIY-transduced mice, developed acute leukemia (two mice) or a preleukemic disorder (one mouse) in the same time frame as recipients of TRAF6-transduced wild-type marrows (**Fig. 5f**, **Supplementary Fig. 10** and **Supplementary Table 8**). These findings suggest that the dysplastic hematopoiesis, cytopenias and thrombocytosis in the TRAF6-chimeric mice are due to a TRAF6-mediated increase in *Il6* expression and resulting paracrine, cell-nonautonomous effects; in contrast, clonal expansion and the propensity to develop acute leukemia are not mediated by IL-6 and are due to cell-autonomous effects of TRAF6 overexpression.

miRNA loss increases megakaryopoiesis via TRAF6 and IL-6

To determine whether knockdown of miR-145 or miR-146a levels results in hematopoietic dysregulation through effects on TRAF6, we used FITC-conjugated locked nucleic acid (LNA) oligonucleotide inhibitors (anti-miRs) to knock down specific target miRNAs in the presence or absence of a dominant-negative TRAF6 construct (**Fig. 5g**). Transfection of anti-miRs into marrow cells resulted in excellent transfection efficiency (**Supplementary Fig. 11a**), ~40% reduction in the amount of the endogenous target miRNA (**Supplementary Fig. 11b**) and target protein derepression (**Supplementary Fig. 11c**). After 48 h in culture, we analyzed the conditioned medium by ELISA for IL-6 protein expression. Knockdown of miR-145 or miR-146a resulted in a threefold or sixfold increase, respectively, of IL-6 expression compared to the scrambled control oligonucleotide (**Fig. 5g**). The increase in IL-6 abundance in the conditioned medium of either miR-145– or miR-146a–knockdown marrow cells was blocked by concurrent transduction of a dominant-negative TRAF6 construct (**Fig. 5g**), indicating that IL-6 induction by miR-145 and miR-146a is routed through a TRAF6 pathway. We also used the conditioned medium to culture wild-type marrow cells for 48 h, followed by quantification of megakaryocyte colonies. Megakaryocyte progenitor activity was increased by ~50% when wild-type marrow cells were cultured in conditioned medium obtained from miR-145– or miR-146a–knockdown cultures (**Fig. 5g**). The increase in megakaryocyte colony formation was abrogated when marrow cells were cultured in conditioned medium obtained from dominant-negative TRAF6–expressing marrow cultures (**Fig. 5g**). This finding suggests a cell-nonautonomous effect of miR-145 and miR-146a on megakaryopoiesis through a TRAF6–IL-6 axis.

To evaluate the individual effects of miR-145 or miR-146a on hematopoiesis, we transplanted marrow cells transfected with anti–miR-145, anti–miR-146a or control LNA-S (scrambled) oligonucleotides into lethally irradiated recipient mice. Marrow collected 5 d after transplant revealed that ~10% of cells retained detectable amounts of anti-miR oligonucleotides (**Supplementary Fig. 11d**). There was a significant increase in megakaryocyte colony formation from the marrow of mice transfected with anti–miR-145 ($P = 0.002$) or anti–miR-146 ($P = 0.0003$) compared to mice transfected with LNA-S (**Supplementary Fig. 11e**). Similarly, flow cytometry revealed an increased proportion of $CD41^+$, but not $Mac1^+$, cells in the marrows and spleens of mice reconstituted with marrow transfected with anti–miR-145 oligonucleotides ($P = 0.09$) or anti–miR-146a oligonucleotides ($P = 0.08$) compared to mice reconstituted with marrow transfected with LNA-S oligonucleotides (**Supplementary Fig. 11f**,**g**).

Increased TIRAP, TRAF6 and IL-6 expression in del(5q) cells

Given that marrow cells from subjects with del(5q) showed low levels of miR-145 and miR-146a (**Fig. 1b**), we expected that these cells would have increased amounts of TIRAP, TRAF6 and IL-6. Immunoblotting showed elevated amounts of TIRAP ($P = 0.0002$) and TRAF6 ($P = 0.0001$) protein in marrow cells from subjects with MDS with del(5q) ($n = 9$) compared to normal age-matched controls ($n = 8$) (**Fig. 5h** and **Supplementary Fig. 12a**,**b**). *IL6* transcript levels, assessed by qRT-PCR, were significantly higher in cells from the subjects with del(5q) compared to controls ($P = 0.03$) (**Fig. 5i**). Thus, loss of a single miR-145 and miR-146a allele correlates with increased expression of TIRAP, TRAF6 and *IL6* in subjects with MDS with del(5q).

DISCUSSION

There is accumulating evidence that miRNA expression is dysregulated in various cancers, including hematological malignancies[24–26]. However, to our knowledge, previous studies have not provided definitive evidence indicating that dysregulation of any miRNA can result in MDS. The commonest structural chromosomal anomaly in individuals with MDS is an interstitial deletion of the long arm of chromosome 5, the isolated deletion of which is associated with a specific MDS subtype called 5q– syndrome[7]. In this report we show reduced expression in bone marrow cells of individuals with del (5q) MDS of two miRNAs—miR-145 and miR-146a—that are abundantly expressed in the $CD34^+$ stem/progenitor fraction of hematopoietic cells and are located within (miR-145) or very close to (miR-146a) the CDR identified in 5q– syndrome[10]. Expression of both miRNAs is markedly reduced in individuals with MDS with del(5q) compared to individuals with MDS without del(5q) or age-matched controls. Levels of miR-145 and miR-146a inversely correlate with their respective target proteins, TIRAP and TRAF6. We thus propose a model in which del(5q) results in haploinsufficiency of miR-145, miR-146a or both. The consequent increased expression of TIRAP and TRAF6 leads to inappropriate activation of innate immune signaling in HSPCs. This activation of the TRAF6-mediated innate immune signaling pathway leads to the megakaryocytic abnormalities observed in individuals harboring del(5q) in HSPCs and the propensity of these individuals to progress to marrow failure and acute leukemia (**Fig. 5j**).

Recent evidence has implicated dysregulation of innate immune signaling in oncogenesis[27–29]. In particular, individuals with cytogenetically normal AML show an miRNA signature that is predicted to result in altered expression of proteins involved in innate immune signaling such as TLR2 and TLR4 (ref. 25). TLR4 has been shown to be upregulated in $CD34^+$ cells from subjects with MDS[30]. Additional correlative data implicating inappropriate innate immune signaling in MDS comes from a study showing a greater than tenfold increase of TRAF6 mRNA levels in $CD34^+$ marrow cells from individuals with MDS relative to normal controls[31] and array comparative genomic hybridization studies showing amplification of genomic regions encompassing TIRAP or TRAF6 in some individuals with MDS[32,33]. Dysregulation of miR-145 and miR-146a has been reported in other hematological malignancies[34–38].

It has been reported that dysplastic cells in MDS are not exclusively part of the chromosomally abnormal clone, suggesting that cell nonautonomous effects contribute to MDS[15,39]. Circulating IL-6 concentrations are elevated in 5q– syndrome and in ~30% of all people with MDS[40–42], and we also found IL-6 mRNA levels to be elevated in subjects with del(5q). IL-6 is a pleotropic cytokine that stimulates megakaryocyte proliferation, colony formation and platelet formation[23]. Relevant to our findings, overexpression of *Il6* in mouse marrow transplantation experiments produces thrombocytosis, anemia and transient neutropenia with progression to leukocytosis[43,44]. We found an inverse correlation between *Il6* and miR-145 or miR-146a expression in marrow cells from individuals

with MDS, and we provide direct evidence that the paracrine effect of TRAF6-induced IL-6 elicits some of the features of 5q– syndrome. Notably, lenalidomide, which is the mainstay of therapy for 5q– syndrome, suppresses expression of IL-6 (ref. 45), suggesting that it may act by inducing miR-145 or miR-146a expression or by inhibiting activation of TRAF6.

Our findings also provide direct evidence that ectopic activation of innate immune signaling by reduced miR-145 and miR-146a expression or enforced expression of TRAF6 in a long-term repopulating cell results in key manifestations of the 5q– syndrome: megakaryocytic dysplasia, elevated platelet counts and mild neutropenia. Long-term TRAF6 expression and inappropriate activation of innate immune signaling also reproduces the natural progression of 5q– syndrome, with a proportion of mice developing marrow failure with severe anemia or AML. Our studies implicate a cell-nonautonomous mechanism for 5q– syndrome–associated megakaryocytic dysplasia, thrombocytosis and cytopenia. However, progression to marrow failure or AML seems to be cell autonomous to TRAF6-expressing cells. Specifically, we find that reduced expression of miR-145 or miR-146a or TRAF6 activation maintains a primitive hematopoietic population and provides prosurvival signals. This model suggests that TRAF6 activation provides an advantage to a primitive HSPC population, thus providing a potential explanation for clonal dominance in MDS. Our observations support a recent finding that transforming growth factor-β–activated kinase-1, a downstream mediator of TRAF6, and TLR4 activation is important for HSPC maintenance[46,47]. Thus, activation of the innate immune pathway through loss of miR-145 or miR-146a recapitulates the natural progression of 5q– syndrome.

Although 5q– syndrome is also defined by macrocytic anemia, we did not observe an erythroid defect in our mouse models. A recent study has reported that partial loss of *RPS14* expression in $CD34^+$ cells by siRNA knockdown results in a severe block of terminal erythroid differentiation and macrocytosis *in vitro*[11]. We therefore speculate that del(5q) results in thrombocytosis and clonal dominance through reduction of miR-145 and miR146a levels and inappropriate activation of innate immune signaling, whereas haploinsufficiency of *RPS14* explains the macrocytic anemia. As *RPS14* and miR-145 are separated by less than one megabase within the CDR, their combined loss may be sufficient to recapitulate virtually all of the major features of 5q– syndrome. The current study provides direct evidence that loss of miR-145 or miR-146a in a long-term repopulating cell results in inappropriate activation of innate immune signaling and the recapitulation of several, but not all, of the major features of 5q– syndrome *in vivo*.

METHODS

Methods and any associated references are available in the online version of the paper at http://www.nature.com/naturemedicine/.

Note: Supplementary information is available on the Nature Medicine website.

ACKNOWLEDGMENTS

We thank R. Deleeuw, R. Chari, W. Lockwood, S. Watson and E. Vucic for technical assistance and helpful discussions and M. Abbott for animal husbandry. K. Tohyama (Kawasaki Medical School) provided the MDS-L cell line. The NF-κB site–containing luciferase reporter plasmid was a gift from F. Jirik (University of Calgary). This work was supported by the Canadian Institutes of Health Research (CIHR; MOP 89976), Leukemia and Lymphoma Society of Canada and Canadian Cancer Society grants to A.K., a CIHR grant and a Terry Fox Foundation Program Project award to R.K.H., and a Stem Cell Network grant to M.M. D.T.S. is supported in part by CIHR and Michael Smith Foundation for Health Research (MSFHR) fellowships. M.M. and A.K. are Senior Scholars of the MSFHR.

AUTHOR CONTRIBUTIONS

D.T.S. and A.K. participated in designing the research and drafting the manuscript; D.T.S. and S.S. performed experiments; F.K., B.A., A.M., and R.M. provided technical assistance and discussion; R.A.W. and R.B. provided human subject samples; D.H. and R.K.H. provided valuable advice and expertise; M.H. and M.M. provided reagents and expertise in small RNA sequencing; W.L. provided valuable reagents and expertise in array comparative genomic hybridization.

Published online at http://www.nature.com/naturemedicine/.
Reprints and permissions information is available online at http://npg.nature.com/reprintsandpermissions/.

1. Corey, S.J. *et al.* Myelodysplastic syndromes: the complexity of stem-cell diseases. *Nat. Rev. Cancer* **7**, 118–129 (2007).
2. Nilsson, L. *et al.* Isolation and characterization of hematopoietic progenitor/stem cells in 5q–deleted myelodysplastic syndromes: evidence for involvement at the hematopoietic stem cell level. *Blood* **96**, 2012–2021 (2000).
3. Nilsson, L. *et al.* The molecular signature of MDS stem cells supports a stem-cell origin of 5q myelodysplastic syndromes. *Blood* **110**, 3005–3014 (2007).
4. Thanopoulou, E. *et al.* Engraftment of NOD/SCID-β2 microglobulin null mice with multilineage neoplastic cells from patients with myelodysplastic syndrome. *Blood* **103**, 4285–4293 (2004).
5. Nimer, S.D. Myelodysplastic syndromes. *Blood* **111**, 4841–4851 (2008).
6. Li, X., Bryant, C.E. & Deeg, H.J. Simultaneous demonstration of clonal chromosome abnormalities and apoptosis in individual marrow cells in myelodysplastic syndrome. *Int. J. Hematol.* **80**, 140–145 (2004).
7. Giagounidis, A.A., Germing, U. & Aul, C. Biological and prognostic significance of chromosome 5q deletions in myeloid malignancies. *Clin. Cancer Res.* **12**, 5–10 (2006).
8. Boultwood, J. *et al.* Narrowing and genomic annotation of the commonly deleted region of the 5q– syndrome. *Blood* **99**, 4638–4641 (2002).
9. Martíinez-Ramirez, A. *et al.* Analysis of myelodysplastic syndromes with complex karyotypes by high-resolution comparative genomic hybridization and subtelomeric CGH array. *Genes Chromosom. Cancer* **42**, 287–298 (2005).
10. Wang, L. *et al.* Genome-wide analysis of copy number changes and loss of heterozygosity in myelodysplastic syndrome with del(5q) using high-density single nucleotide polymorphism arrays. *Haematologica* **93**, 994–1000 (2008).
11. Ebert, B.L. *et al.* Identification of RPS14 as a 5q– syndrome gene by RNA interference screen. *Nature* **451**, 335–339 (2008).
12. Bartel, D.P. MicroRNAs: genomics, biogenesis, mechanism and function. *Cell* **116**, 281–297 (2004).
13. Ebert, M.S., Neilson, J.R. & Sharp, P.A. MicroRNA sponges: competitive inhibitors of small RNAs in mammalian cells. *Nat. Methods* **4**, 721–726 (2007).
14. Gentner, B. *et al.* Stable knockdown of microRNA *in vivo* by lentiviral vectors. *Nat. Methods* **6**, 63–66 (2009).
15. Bigoni, R. *et al.* Multilineage involvement in the 5q– syndrome: a fluorescent *in situ* hybridization study on bone marrow smears. *Haematologica* **86**, 375–381 (2001).
16. Kroef, M.J. *et al.* Mosaicism of the 5q deletion as assessed by interphase FISH is a common phenomenon in MDS and restricted to myeloid cells. *Leukemia* **11**, 519–523 (1997).
17. Lewis, B.P., Shih, I.H., Jones-Rhoades, M.W., Bartel, D.P. & Burge, C.B. Prediction of mammalian microRNA targets. *Cell* **115**, 787–798 (2003).
18. Taganov, K.D., Boldin, M.P., Chang, K.J. & Baltimore, D. NF-κB–dependent induction of microRNA miR-146, an inhibitor targeted to signaling proteins of innate immune responses. *Proc. Natl. Acad. Sci. USA* **103**, 12481–12486 (2006).
19. Lamothe, B. *et al.* Site-specific Lys-63-linked tumor necrosis factor receptor–associated factor 6 auto-ubiquitination is a critical determinant of I κ B kinase activation. *J. Biol. Chem.* **282**, 4102–4112 (2007).
20. Mansell, A., Brint, E., Gould, J.A., O'Neill, L.A. & Hertzog, P.J. Mal interacts with tumor necrosis factor receptor-associated factor (TRAF)-6 to mediate NF-κB activation by Toll-like receptor (TLR)-2 and TLR4. *J. Biol. Chem.* **279**, 37227–37230 (2004).
21. Wang, C. *et al.* TAK1 is a ubiquitin-dependent kinase of MKK and IKK. *Nature* **412**, 346–351 (2001).
22. Nimer, S.D. Clinical management of myelodysplastic syndromes with interstitial deletion of chromosome 5q. *J. Clin. Oncol.* **24**, 2576–2582 (2006).
23. Kishimoto, T. Interleukin-6: from basic science to medicine—40 years in immunology. *Annu. Rev. Immunol.* **23**, 1–21 (2005).
24. Garzon, R. *et al.* MicroRNA signatures associated with cytogenetics and prognosis in acute myeloid leukemia. *Blood* **111**, 3183–3189 (2008).
25. Marcucci, G. *et al.* MicroRNA expression in cytogenetically normal acute myeloid leukemia. *N. Engl. J. Med.* **358**, 1919–1928 (2008).
26. Takada, S. *et al.* MicroRNA expression profiles of human leukemias. *Leukemia* **22**, 1274–1278 (2008).
27. Rakoff-Nahoum, S. & Medzhitov, R. Regulation of spontaneous intestinal tumorigenesis through the adaptor protein MyD88. *Science* **317**, 124–127 (2007).

28. Bhaumik, D. *et al.* Expression of microRNA-146 suppresses NF-κB activity with reduction of metastatic potential in breast cancer cells. *Oncogene* **27**, 5643–5647 (2008).
29. Chen, H. *et al.* Interference with nuclear factor κ B and c-Jun NH2-terminal kinase signaling by TRAF6C small interfering RNA inhibits myeloma cell proliferation and enhances apoptosis. *Oncogene* **25**, 6520–6527 (2006).
30. Maratheftis, C.I., Andreakos, E., Moutsopoulos, H.M. & Voulgarelis, M. Toll-like receptor-4 is up-regulated in hematopoietic progenitor cells and contributes to increased apoptosis in myelodysplastic syndromes. *Clin. Cancer Res.* **13**, 1154–1160 (2007).
31. Hofmann, W.K. *et al.* Characterization of gene expression of CD34$^+$ cells from normal and myelodysplastic bone marrow. *Blood* **100**, 3553–3560 (2002).
32. Gondek, L.P. *et al.* Chromosomal lesions and uniparental disomy detected by SNP arrays in MDS, MDS/MPD and MDS-derived AML. *Blood* **111**, 1534–1542 (2008).
33. Starczynowski, D.T. *et al.* High-resolution whole genome tiling path array CGH analysis of CD34$^+$ cells from patients with low-risk myelodysplastic syndromes reveals cryptic copy number alterations and predicts overall and leukemia-free survival. *Blood* **112**, 3412–3424 (2008).
34. Garzon, R. *et al.* Distinctive microRNA signature of acute myeloid leukemia bearing cytoplasmic mutated nucleophosmin. *Proc. Natl. Acad. Sci. USA* **105**, 3945–3950 (2008).
35. Garzon, R. *et al.* MicroRNA signatures associated with cytogenetics and prognosis in acute myeloid leukemia. *Blood* **111**, 3183–3189 (2008).
36. Jongen-Lavrencic, M., Sun, S.M., Dijkstra, M.K., Valk, P.J. & Lowenberg, B. MicroRNA expression profiling in relation to the genetic heterogeneity of acute myeloid leukemia. *Blood* **111**, 5078–5085 (2008).
37. Li, Z. *et al.* Distinct microRNA expression profiles in acute myeloid leukemia with common translocations. *Proc. Natl. Acad. Sci. USA* **105**, 15535–15540 (2008).
38. Takada, S. *et al.* MicroRNA expression profiles of human leukemias. *Leukemia* **22**, 1274–1278 (2008).
39. Hast, R., Eriksson, M., Widell, S., Arvidsson, I. & Bemell, P. Neutrophil dysplasia is not a specific feature of the abnormal chromosomal clone in myelodysplastic syndromes. *Leuk. Res.* **23**, 579–584 (1999).
40. Herold, M., Schmalzl, F. & Zwierzina, H. Increased serum interleukin 6 levels in patients with myelodysplastic syndromes. *Leuk. Res.* **16**, 585–588 (1992).
41. Verhoef, G.E. *et al.* Measurement of serum cytokine levels in patients with myelodysplastic syndromes. *Leukemia* **6**, 1268–1272 (1992).
42. Hsu, H.C. *et al.* Circulating levels of thrombopoietic and inflammatory cytokines in patients with acute myeloblastic leukemia and myelodysplastic syndrome. *Oncology* **63**, 64–69 (2002).
43. Brandt, S.J., Bodine, D.M., Dunbar, C.E. & Nienhuis, A.W. Dysregulated interleukin 6 expression produces a syndrome resembling Castleman's disease in mice. *J. Clin. Invest.* **86**, 592–599 (1990).
44. Hawley, R.G., Fong, A.Z., Burns, B.F. & Hawley, T.S. Transplantable myeloproliferative disease induced in mice by an interleukin 6 retrovirus. *J. Exp. Med.* **176**, 1149–1163 (1992).
45. Corral, L.G. *et al.* Differential cytokine modulation and T cell activation by two distinct classes of thalidomide analogues that are potent inhibitors of TNF-α. *J. Immunol.* **163**, 380–386 (1999).
46. Nagai, Y. *et al.* Toll-like receptors on hematopoietic progenitor cells stimulate innate immune system replenishment. *Immunity* **24**, 801–812 (2006).
47. Tang, M. *et al.* TAK1 is required for the survival of hematopoietic cells and hepatocytes in mice. *J. Exp. Med.* **205**, 1611–1619 (2008).

ONLINE METHODS

Sample collection and cell lines. We obtained bone marrow samples under informed consent from subjects diagnosed with MDS under protocols approved by the Institutional Review Boards of the British Columbia Cancer Agency and Sunnybrook Research Institute. We purchased AML cell lines KG-1, KG-1a, UT-7 and THP-1 from American Type Culture Collection. The nonleukemic myelodysplastic cell line, MDS-L, was obtained from K. Tohyama.

microRNA isolation and expression analysis. We isolated the small RNA fraction with the mirVana Paris Isolation kit (Ambion). We quantified miRNA expression with the mirVana qRT-PCR miRNA Detection Kit (Ambion) or stem-loop primers. We used the small RNA fraction for reverse transcription using reverse transcription primers specific for each miRNA (**Supplementary Table 9**). We subsequently used the complementary DNA synthesis reaction for quantitative or semiquantitative PCR with miRNA-specific primers (**Supplementary Table 9**). Additional details are provided in the **Supplementary Methods**. For semiquantitative PCR, we visualized bands on a 3% high-purity agarose gel. We determined the relative expression of miRNAs by densitometry.

Retroviral vectors, packaging cell lines and bone marrow transplantation. We fused miRNA decoy sequences (tandem repeats complementary to miR-145 and miR-146a) to the 3′ UTR of the *YFP* cDNA and then cloned them into the dual promoter phosphoglycerate retroviral vector. Sequence information for the miRNA decoy is provided in the **Supplementary Methods**. We cloned Flag-TRAF6 into the MIY retroviral vector[48]. We performed virus packaging and infection of ecotropic packaging cell lines (GP^+E86)[48] as previously described[49]. We carried out bone marrow transplantation studies using protocols[49] approved by the University of British Columbia Animal Care Committee (**Supplementary Methods**).

Peripheral blood and bone marrow analysis. We monitored donor-derived engraftment and reconstitution by flow cytometric analysis of YFP expression in the peripheral blood. For immunophenotypic analysis, we washed and resuspended bone marrow cells or peripheral blood in PBS containing 4% goat serum, followed by primary monoclonal antibody (phycoerythrin (PE)- or allophycocyanin-labeled) staining overnight. Antibodies are described in the **Supplementary Methods**. We obtained mouse marrow progenitors by depleting Lin^+ cells by magnetic separation (Stem Cell Technologies). We ran samples on a FACScalibur flow cytometer (Beckman Coulter) and analyzed data with FlowJo (version 8.7, TreeStar). We performed complete blood counts on the peripheral blood using Scil Vet ABC Hematology Analyzer (Scil Animal Care Company). Blood counts obtained between 2 and 3 months after transplantation for all mice are shown in **Supplementary Tables 3**, **4** and **7**. We performed cytospins at the time of bone marrow collection and subsequently stained the cells with Wright-Giemsa using Hema-Tek Slide Stainer (Miles). We fixed organs and tissues in PBS with 4% paraformaldehyde, paraffin-embedded them, sectioned them and stained them with H&E.

Luciferase assay. pcDNA-hsa-miR-146a, pMirReport-TRAF6-3′UTR (wild-type) and pMirReport-TRAF6-3′UTR (mutant) are described elsewhere[18]. We synthesized and cloned hsa–miR-145 into pcDNA and hTIRAP 3′ UTR (wild-type) and hTIRAP 3′ UTR (mutant) into pMirReport. We inserted a 64–base pair fragment of the TIRAP 3′ UTR encompassing the single miR-145 target site or a ~500–base pair fragment of the TRAF6 3′ UTR encompassing two miR-146a target sites downstream of the open reading frame of the luciferase reporter gene. We purchased LNA oligonucleotides (FITC-conjugated) for knockdown of miR-143 (anti–miR-143, 5′-GAGCTACAGTGCTTCATCTCA-3′), miR-145 (anti–miR-145, 5′-AGGGATTCCTGGGAAAACTGGAC-3′), miR-146a (anti–miR-146, 5′-AACCCATGGAATTCAGTTCTCA-3′) and a scrambled control oligonucleotide (LNA-S, 5′-GTGTAACACGTCTATACGCCCA-3′) from Exiqon. For the 3′ UTR luciferase assays, we transfected 250 ng of pMirReport-3′ UTR, 250 ng of pcDNA or pcDNA-miR, 10 ng of thymidine kinase–driven *Renilla* luciferase and 100 nM of LNA into HEK293 cells (12-well format) using TransiT transfection reagent (Mirus). For NF-κB activation assays in NIH3T3 cells, we used an NF-κB site–containing luciferase reporter plasmid (300 ng) (gift from F. Jirik).

Preparation of cDNA and reverse-transcription PCR of mRNA. We extracted total cellular RNA with Trizol reagent (Invitrogen). We used the purified total RNA preparation as a template to generate first-strand cDNA synthesis using SuperScript II (Invitrogen).

Clonogenic progenitor assay. We determined hematopoietic clonogenic progenitor frequencies by plating 1×10^3 marrow cells in methylcellulose medium containing human erythropoietin, mouse stem cell factor, mouse IL-3 and human IL-6 (Methocult GF M3434; Stem Cell Technologies). We scored colonies after 10 d. For megakaryocyte clonogenic progenitor frequencies, we plated 1×10^4 marrow cells in collagen-based medium containing mouse IL-3, human IL-6 and human thrombopoietin (MegaCult, StemCell Technologies). We fixed, dried and stained slides according to the manufacturer's recommendations.

Enzyme-linked immunosorbent assay. We plated marrow cells in a 35-mm culture dish at a density of ~500,000 cells and cultured them for 24 h. We recovered the supernatants and centrifuged them (850*g*, 10 min). For mouse serum analysis, we collected blood from the mice and allowed it to clot overnight at 4 °C. After centrifugation (850*g*, 10 min) we recovered the serum. We determined murine IL-6, IL-1β and tumor necrosis factor-α concentrations by standard sandwich ELISA, according to the manufacturer's (Ebiosciences) instructions.

DNA ploidy analysis. We washed bone marrow cells in PBS containing 4% goat serum, followed by incubation in 70% ethanol overnight. After washing in PBS, we stained the cells for 30 min in primary nonoclonal antibody: PE-Cy5–conjugated antibody to mouse CD41 (clone MWReg30, Pharmingen) or PE-Cy5–conjugated antibody to mouse CD61 (2C9.G2, Pharmingen). We added 1 μg ml^{-1} propidium iodine to the cells for 15 min and then analyzed them by FACS. We evaluated megakaryocyte DNA ploidy by gating on $CD41^+$ or $CD61^+$ cells and measuring propidum iodide incorporation. Data are presented as $CD41^+$ or $CD61^+$ cells that contain less than 4*n* DNA. The gates for ploidy analysis were established on $CD41^-$ or $CD61^-$ cells.

Statistical analyses. Results are depicted as the means ± s.e.m. We performed statistical analyses with Student's *t*-test. We applied a correction for multiple testing (Benjamini and Hochberg) to the data in **Figure 1b**. We compared survival between groups by the Kaplan-Meier test, and we calculated *P* value by the log-rank test. We used box-and-whisker plots in **Figures 1b** and **2c** to depict the range and percentiles of values obtained. We used GraphPad Prism (v4, GraphPad) for statistical analyses.

Additional methods. Detailed methodology is described in the **Supplementary Methods**.

48. Antonchuk, J., Sauvageau, G. & Humphries, R.K. HOXB4-induced expansion of adult hematopoietic stem cells *ex vivo*. *Exp. Hematol.* **29**, 1125–1134 (2001).
49. Larrivée, B., Pollet, I. & Karsan, A. Activation of vascular endothelial growth factor receptor-2 in bone marrow leads to accumulation of myeloid cells: role of granulocyte-macrophage colony-stimulating factor. *J. Immunol.* **175**, 3015–3024 (2005).